ANALYSIS OF GISP2 BEDROCK COSMOGENIC-NUCLIDE DATA: Supplement to "GISP2 bedrock reveals extended periods of ice-free Greenland during the Pleistocene" by Schaefer and others

---

Summary: This document describes how we infer information about the exposure history of GISP2 subglacial bedrock from the measured ^{26}Al and ^{10}Be concentrations. First, we discuss the variation in cosmogenic-nuclide concentrations with depth in the core. The fact that nuclide concentrations decrease with depth requires that they are the result of cosmic-ray production near the surface, and the form of the depth-concentration relationship allows us to quantify where the samples were in relation to the Earth's surface during cosmic-ray exposure. Second, we explore a series of hypothetical exposure histories to determine which are and are not consistent with all the observations, including the absolute ^{26}Al and ^{10}Be concentrations, the depth-dependence of the concentrations, and the ^{26}Al/^{10}Be ratios.

In principle, there exist an infinite number of potential exposure histories that are consistent with a given set of ^{26}Al and ^{10}Be measurements. Thus, it is not possible to invert our observations to yield a single unique exposure history, or by extension a single best-fitting ice sheet change history. Instead, we use the approach of proposing a number of broad classes of exposure histories and asking if they can be fit to the observations. For example, if we propose that the observations can be explained by a single period of surface exposure followed by a single period of ice cover, we can ask whether there exist any values for the exposure and burial durations that provide an acceptable fit to the observations. If no such values exist, this class of exposure histories is not consistent with the observations. If such values do exist, they define exposure histories that are consistent with the observations and thus could potentially represent the true exposure history of the site.

We will use this reasoning to support three main conclusions. First, although the present bedrock surface in the core must have been covered by some additional rock, soil, or ice during past periods of cosmic-ray exposure, the thickness of this material cannot have been more than a few meters. Thus, the observations require the absence of the Greenland Ice Sheet during periods of cosmic-ray exposure. Second, the longest possible length of time that the present ice sheet could have remained continuously present at the core site is approximately 1.1 million years. Third, although there exist many paleoclimatically plausible scenarios of ice sheet change that are consistent with the observations, all these scenarios require the absence of the ice sheet at the core site during some or all Pleistocene interglaciations.

1. What was measured. We combined core segments to yield enough quartz for ^{10}Be or ^{26}Al measurements (see Fig. 2); for ^{26}Al, more segments were combined for each analysis, leading to fewer analyses than for ^{10}Be. In some cases core segments were discontinuous. Figure S1 shows this. We are not including in this analysis a preliminary ^{26}Al measurement from the lowest core segments, because the Al yield in the extraction chemistry could not be verified and ^{26}Al/^{27}Al measurement was close to detection limits.

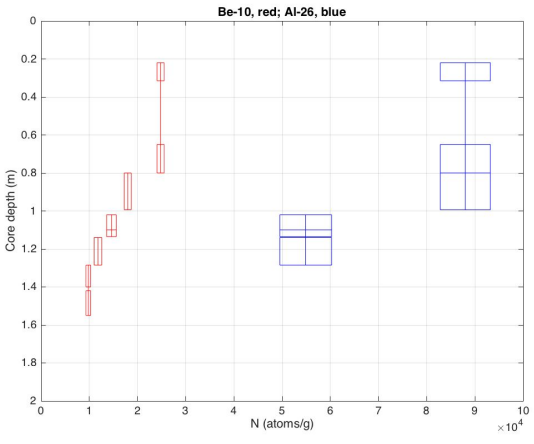

Figure S1. ^{10}Be (red) and ^{26}Al (blue) concentrations in GISP2 bedrock core segments. These data are also shown in Figure 2 in the main text. Each box corresponds to a core segment. The box height indicates the vertical thickness of each segment; vertical lines connect core segments that were amalgamated for each analysis. In most cases amalgamated segments were adjacent to each other (in which case multiple boxes are likewise adjacent), but in some cases they were separated by gaps in core recovery. Note that this figure does not imply that the ^{10}Be concentrations at 0.3 and 0.7 m, for example, are the same; it shows the average value for an amalgamated sample that includes two separate core segments from those depths. Width of boxes shows measurement uncertainty (1-sigma).

2. Basic observations. The three basic observations about these data, which we will explore and quantify in the subsequent discussion, are: (i) cosmogenic-nuclide concentrations decrease with depth in the core; (ii)

concentrations decrease less rapidly than we would expect if the bedrock surface in the core had been the land surface during exposure; and (iii) the measured $^{26}Al/^{10}Be$ ratio in these samples is substantially less than the surface production ratio of 6.75.

3. Depth-dependence of cosmogenic-nuclide concentrations. Production of ^{10}Be and ^{26}Al occurs both by high-energy neutron spallation and by muon interactions. At and immediately below the surface, most production is by spallation, and spallogenic production rates decrease exponentially with depth with an *e*-folding length near 140 g/cm^2 (this value is appropriate for high latitude). With increasing depth, spallogenic production becomes less important than production due to deeply penetrating muons, which has a longer *e*-folding length (> 1500 g/cm^2, increasing with depth). A single exponential curve fit to the observed concentrations has an an *e*-folding length intermediate between these two (specifically, 262 g/cm^2, although because a single exponential function does not fit the data adequately, this value is not physically meaningful). Thus, the observed nuclide concentrations reflect both spallogenic and muon production. In other words, the observations are not consistent with a single period of exposure during which the present bedrock surface was the land surface (in this case the measured concentrations would decrease with an *e*-folding length near 140 g/cm^2). The fact that we observe an apparent *e*-folding length that is longer than expected for spallogenic production alone requires that a significant fraction of the measured nuclide concentrations is the result of production by muons, which means that production took place farther below the surface than the samples are now below the bedrock surface. The data are also not consistent with exposure more than a few meters below the surface (in which case the contribution from spallogenic production would be negligible, and the concentrations would decrease with an e-folding length characteristic of muon production).

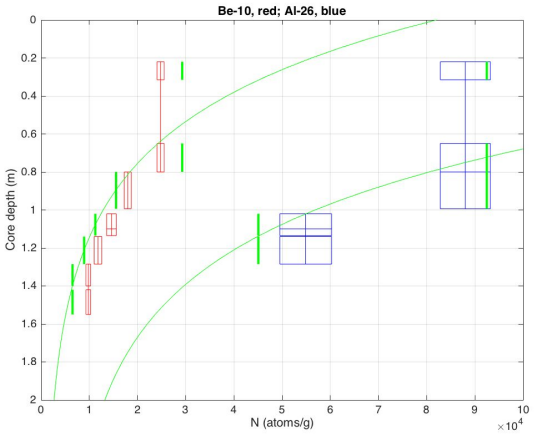

Figure S2. Observed ^{10}Be and ^{26}Al concentrations compared to production profiles (including both spallogenic and muon-induced production; see details below) under the assumption that the bedrock surface was the land surface at the time that exposure took place. Here we attempt to fit the observations by assuming zero erosion and varying the exposure durations for ^{10}Be and ^{26}Al (we treat these separately at present, that is, they are not forced to obey the production ratio. We address this issue later). Solid green lines are production profiles for ^{10}Be and ^{26}Al. In this and subsequent figures, vertical green bars are production rates averaged over depth ranges corresponding to each analysis of amalgamated core segments; thus, the green bar is the model prediction we are comparing to the observations.

Figure S2 shows that the depth dependence of the production rate immediately below the surface has a much shorter *e*-folding length than the depth dependence of the measured nuclide concentrations. In other words, an exposure model including a period of surface exposure, with negligible erosion, during which time the bedrock surface was the land surface, does not fit the data.

Figure S3 then shows the result of assuming that the bedrock surface was covered by some additional mass during the period of exposure. In other words, we are trying to fit the measurements to the production profile by adjusting how far the bedrock surface was below the actual land surface at the time that exposure took place. We represent this by an additional mass cover thickness covering the bedrock surface. The best-fitting cover thickness, the fit of which is shown in Figure 2 in the main text and here in Figure S3, is 350 g/cm^2. A nominal uncertainty on this value derived only from the measurement uncertainties (using a Monte Carlo estimate) is ± 20 g/cm^2. However, the best-fitting cover thickness also depends on the assumed mean atmospheric pressure at the site during exposure (which, as discussed in more detail below, is not well constrained), because this affects the relative proportion of spallogenic and muon-induced production. For example, reducing the atmospheric pressure by 25 hPa (equivalent to an increase in site elevation of ca. 200 m) would imply a best-fitting cover thickness of 375 g/cm^2 instead of 350. Thus, the nominal measurement uncertainty of 20 g/cm^2 is not physically meaningful.

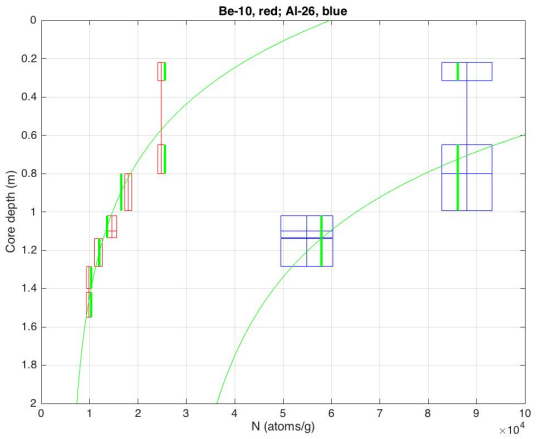

Figure S3. Observed ^{10}Be and ^{26}Al concentrations fit to a production profile by adjusting the depth of the bedrock surface beneath the land surface as well as the exposure duration. The fitting procedure is the same as described above for Figure S2, except that we add the cover thickness as an additional fitting parameter. The best-fit cover thickness is 350 g/cm^2. Again, the thin green lines are continuous representations of the production rate - depth relationship, and the thick green bars are average production rates corresponding to the core segments analysed. This is also shown in Figure 2 in the main text.

350 g/cm^2 of mass thickness is approximately 1.3 m of rock, 1.7 m of soil, or 3.8 m of ice. Thus, the simplest explanation for the observed depth-dependence of the measured nuclide concentrations is that the bedrock surface was covered by 1-4 m of soil, sediment, rock, or ice when exposure took place. Later, for completeness, we consider a more complicated and geologically less likely potential explanation involving a long period of continuous surface exposure at a relatively high erosion rate, and show that it does not provide as good a fit to the measurements.

Although the depth-dependence of the measured nuclide concentrations shows that the present bedrock surface was likely covered by some additional shielding at the time of nuclide production, it is important to note that it also requires that production took place within a few meters of the Earth's surface. Specifically, the observed nuclide inventory could not be the result of long residence under tens or hundreds of meters of ice; in this case, nuclide concentrations would decrease less with depth.

4. Forward model calculations for proposed exposure-burial histories. We now proceed by developing a forward model to compute the predicted nuclide concentrations in our samples given a specified exposure history.

First, we describe our production rate calculations in detail. These also apply to the calculations above in Figures S2 and S3. We assume a reference ^{10}Be production rate due to spallation of 4.1 atoms/g/yr, which follows Balco et al. (2009) but is adjusted for the difference in muon interaction cross sections between those used here and those used in that work; a ^{26}Al/^{10}Be production ratio of 6.75 (Balco et al., 2008); and the production rate scaling method of Stone (2000), as implemented in Balco et al. (2008). We assume that the land surface at the core site during periods of exposure is located at sea level, and compute the atmospheric pressure using the spatially variable atmosphere of Balco et al. (2008). Note that this is speculative because both the elevation of the site and the atmospheric pressure distribution would most likely be very different in the absence of the Greenland Ice Sheet; in addition, both would experience transient changes during ice-free periods. We take the ^{10}Be decay constant to be 4.99 x 10^{-7} (Chmeleff et al., 2010; Korschinek et al., 2010) and the ^{26}Al decay constant to be 9.83 x 10^{-7} (Nishiizumi, 2004). We compute production rates due to muons using the MATLAB implementation in Balco et al. (2008) of the method of Heisinger et al. (2002a,b). However, we use muon interaction cross-sections derived from fitting this method to measurements from a deep sandstone core in Antarctica. These measurements are reported in Borchers et al (2015); the fitted cross-sections are: for ^{10}Be, f^* = 0.0011 and σ_0 = 0.81 μb; for ^{26}Al, f^* = 0.0084 and σ_0 = 13.6 μb (these symbols correspond to those used by Heisinger et al.). These differ from the values given in Phillips et al. (2016), because we are using different code to compute the muon fluxes. Note that our main conclusions in this paper relate to the duration of ice cover of the site, which is sensitive to the values we use for the ^{10}Be and ^{26}Al decay constants and the ^{26}Al/^{10}Be production ratio, but is insensitive to inaccuracies in the absolute magnitude of the production rates. This is important because the uncertainty in our knowledge of the elevation and atmospheric pressure prevailing at the site during ice-free periods means that we are unlikely to be accurately estimating surface production rates when past exposure took place.

We now describe the model calculation of the nuclide concentrations expected for a particular exposure history. Assuming an exposure history is equivalent to specifying the mass cover thickness z_c (mass thickness has units of g/cm^2) above the surface of the bedrock in the core at all past time. We define a time coordinate t that is zero at the present time and positive for past times, and then define an exposure history as a function $z_c(t)$ that describes the variation in z_c over time. For example, if the exposure history consists of one period of surface exposure followed by

one period of cover by the full thickness of the Greenland ice sheet, then $z_c(t)$ equals zero during the period of exposure and is effectively infinite (order 100 m ice thickness or greater is effectively infinite burial, that is, zero cosmogenic-nuclide production) during the period of ice cover. Another example is that surface erosion during ice-free periods would be represented by $z_c(t)$ steadily decreasing during the ice-free period at the rate of erosion.

Given an exposure history $z_c(t)$, then, and also knowing the production rate of nuclide k as a function of mass depth z, $P_k(z)$ (atoms/g/yr; calculated as described above), the predicted average concentration $N_{j,k}$ (atoms/g) of nuclide k in sample j at the present time is then given by the integral:

$$N_{j,k} = (z_{j,bottom} - z_{j,top})^{-1} \int_{z_{j,top}}^{z_{j,bottom}} \int_0^{t_{max}} P_k\left(\zeta + z_c(\tau)\right) \exp\left(-\lambda_k \tau\right) d\tau d\zeta \qquad (1)$$

Where $z_{j,bottom}$ and $z_{j,top}$ are the top and bottom mass depths (g/cm^2) of sample j below the bedrock surface, $z_c(t)$ is the exposure history, that is, the mass thickness (g/cm^2) covering the bedrock surface as a function of time t (yr), λ_k is the decay constant (1/yr) of nuclide k, and τ and ζ are variables of integration. As noted above, the time coordinate is defined to be zero at the present time and positive for past times: t_{max} is the time that the exposure history begins, and the nuclide concentration at t_{max} is zero. In the case that the sample is composed of multiple core segments, we evaluate the integral for each segment separately and then calculate the average nuclide concentration in the combined sample according to the weight of quartz contributed to the analysis by each subsample. We evaluate this integral using the default numerical integration routine in MATLAB software with, for computational efficiency, a piecewise-linear approximation of $P_k(z)$ defined on a logarithmic grid. The MATLAB code used for these calculations is part of this publication and also available at:

http://noblegas.berkeley.edu/~balcs/transfer/GISP2

The misfit statistic we use in comparing predicted to measured nuclide concentrations is the chi-squared statistic using the measurement uncertainty in the nuclide concentrations as the weighting. It is important to note that because the measurement uncertainties for ^{10}Be are significantly smaller than those for ^{26}Al, this statistic assigns greater importance to the ^{10}Be measurements and is more sensitive to whether the model matches the depth profile of ^{10}Be concentrations than to whether the model matches ^{26}Al/^{10}Be ratios. A fit statistic that weighted the ^{26}Al data set equally with the ^{10}Be data set might yield slightly different conclusions, although we tested this and did not find a significant effect on the main conclusions of the paper.

Another important point about the fit statistic is that we assume that the measured core depths and density are exact. This is unlikely to be strictly true, because the core is jointed and somewhat fragmented, with short missing sections, as shown in Figure 1 in the main text, and small vertical displacements of the core segments during recovery are likely. Thus, the probabilities-of-fit to the observations discussed below most likely underestimate the model performance; if we accounted for additional uncertainties in depth and density we would obtain higher probabilities-of-fit.

5. Model 1: simple exposure-burial, sediment cover, zero erosion. Several observations lead us to the simplest possible exposure history that can potentially explain our data. By "simplest," we mean the exposure history that has the fewest distinct periods of surface exposure or burial by the ice sheet. First, the fact that we observe significant cosmogenic-nuclide concentrations that decrease with depth indicates that a period of surface exposure occurred. Second, the depth-dependence of the concentrations, as discussed above, indicates that the bedrock surface was most likely shielded by additional cover at the time that exposure took place. Third, the fact that the observed ^{26}Al/^{10}Be ratio is lower than the surface production ratio indicates that the samples have been shielded from the surface cosmic-ray flux, presumably by the present Greenland Ice Sheet, for some time. We illustrate this in Figure S4 by plotting ^{26}Al and ^{10}Be concentrations, for the two samples in which we measured both ^{10}Be and ^{26}Al, on a [^{10}Be] - [^{26}Al]/[^{10}Be] diagram. We compute these ^{10}Be concentrations by averaging the measured ^{10}Be concentrations in subsamples according to the weight of quartz contributed by each subsample (Extended Data Table 1).

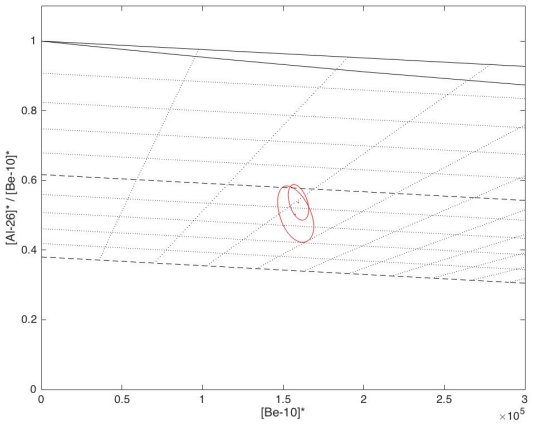

Figure S4. [^{10}Be] - [^{26}Al]/[^{10}Be] diagram for two amalgamated core samples in which both ^{10}Be and ^{26}Al were measured. Measured concentrations have been normalized by production rates calculated assuming that the bedrock surface was covered by 350 g/cm^2 of additional shielding during exposure (see discussion above). The solid black lines are the simple exposure region. Darker dashed lines are isolines of burial in increments of 1 Ma; lighter dotted lines are isolines of burial in 0.2 Ma increments and isolines of exposure time in 0.1 Ma increments. Red ellipses are 68% confidence regions including measurement uncertainties only. This figure also appears in Figure 2 as Panel C in the main text.

These three observations show that the simplest possible exposure model that can explain our observations must include at least one period of surface exposure, at least one period of burial, and some thickness of additional cover of the bedrock surface. For the time being we assume zero surface erosion at all times. We now fit a model with these three parameters to the observations.

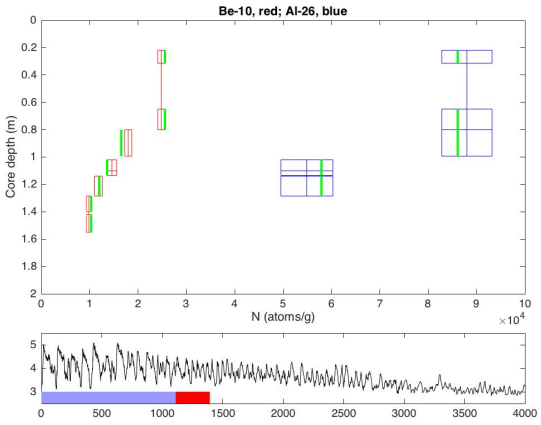

Figure S5 (left). Green lines in the upper panel show predicted concentrations for the best-fitting exposure model with three adjustable parameters -- length of a single period of exposure with no erosion, length of a single period of burial, and mass thickness of cover of bedrock surface. The lower panel shows the LR04 marine benthic oxygen isotope stack (Lisiecki and Raymo, 2005) with the exposure history represented as red (ice-free periods) and blue (ice-covered) bars.

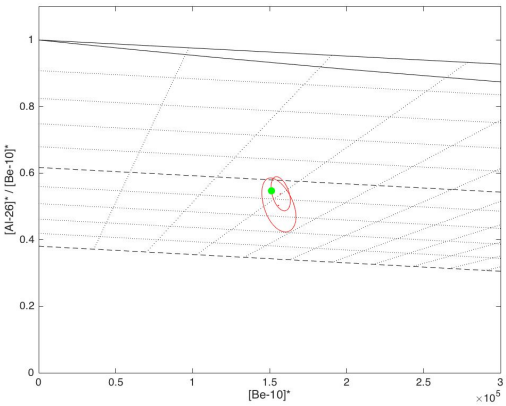

Figure S6. Nuclide concentrations predicted by the best-fit exposure history shown in Figure S5, on the two-nuclide plot of Figure S4. Green dot shows concentrations predicted by the model in Figure S5. Note that we are fitting to all ^{26}Al and ^{10}Be measurements, not just the two paired measurements shown here.

Figures S5 and S6 show the results of fitting a model with these three adjustable parameters -- the duration of a single period of exposure; the duration of a subsequent period of burial; and the cover thickness above the present bedrock surface -- to the observations.

This model fits the observations with reduced chi-squared of 1.9 for 4 degrees of freedom (DOF), which is a probability of fit of 0.11. Given that the probability-of-fit is likely biased low as discussed above, we view this as an acceptable fit. As discussed above, note that the fitting statistics here are disproportionately affected by whether or not the depth profile fits the relatively high-precision ^{10}Be measurements; because the model is overparameterized in relation to a single ^{26}Al/^{10}Be pair, the exposure time and burial time parameters could be chosen to exactly fit either pair. The best-fitting exposure history here has 280 ka of exposure under 350 g/cm^2 of additional cover, followed by 1.1 Ma burial. A Monte Carlo uncertainty analysis considering only measurement uncertainties indicates formal

uncertainties in these parameters as follows: exposure time 282 +/- 31 ka; burial time 1.110 +/- 0.092 Ma. If we include uncertainties in decay constants, the uncertainty on the burial time is 0.109 Ma. Note that these uncertainties only apply if Model 1 is assumed to be correct *a priori*. In reality, of course, although Model 1 is consistent with the cosmogenic-nuclide measurements taken by themselves, geological and paleoclimate considerations show that it is unlikely. In addition, the best-fitting exposure duration for this model is also somewhat dependent on the assumed atmospheric pressure. For example, decreasing the assumed atmospheric pressure by 25 hPa (as we did above in the discussion of cover thickness; approximately equivalent to a 200 m increase in elevation) decreases the best-fitting exposure duration by 6 ka (to 276 ka) . Note, however, that this does not affect the estimate of burial duration.

This calculation highlights the fact that because of the additional cover thickness that we need to match the attenuation length, the exposure time must be relatively long to account for the observed nuclide concentrations. At face value, the measured nuclide concentrations are similar to typical surface concentrations in modern deglaciated landscapes that have experienced only on the order of 10,000 years of Holocene surface exposure. However, because exposure took place below the land surface (below 1.3 m of rock, 1.7 m of soil or 3.4 m of ice, see above), they actually record an exposure history that is much longer than a single interglacial, or even a few interglacials.

6. Model 2: steady-state erosion followed by burial. Another theoretical explanation for the fact that the depth-dependence of the measured concentrations cannot be explained by spallogenic production alone would be a scenario in which the bedrock surface had been allowed to erode at a steady rate for a long period of time. A long period of steady erosion means that a large fraction of the near-surface nuclide inventory was actually produced at depth by muons, and has been brought to the surface by erosion. This results in a longer apparent attenuation length near the surface than expected for spallogenic production only. In effect, steady erosion acts to drag the lower, longer-attenuation-length, part of the profile towards the surface. This scenario is unlikely for geological and paleoclimatic reasons because it takes a long period of steady erosion for the muon-produced inventory to reach steady state. For example, at 30 m/Myr, (see below) it would take on the order of 1 Myr of continuous exposure and steady erosion for the muon-produced ^{10}Be inventory to reach steady state. In other words, although the steady-state scenario removes the need for additional sediment cover of the bedrock surface, it requires a very long period of undisturbed exposure prior to burial. In any case, we consider it here for completeness.

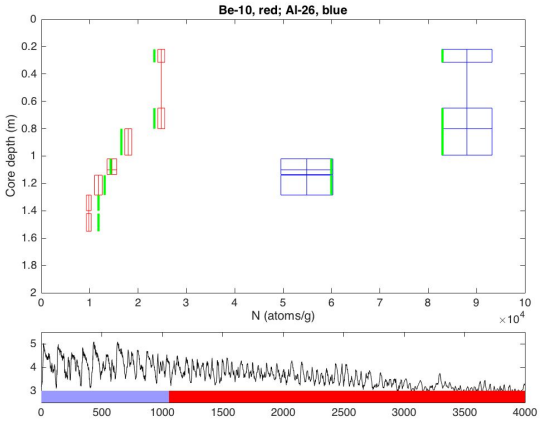

Figure S7. Best-fitting model with no cover of the bedrock surface and steady-state erosion followed by a single period of burial at infinite depth.

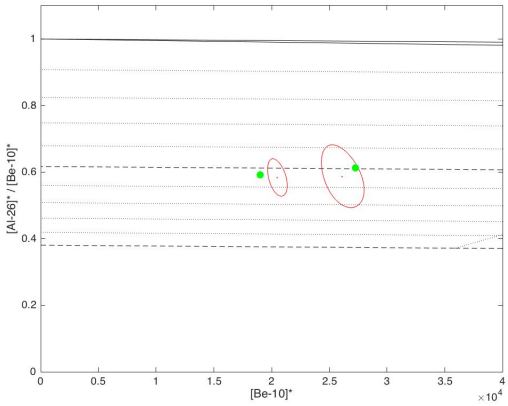

Figure S8. Same exposure history as in Figure S7 on two-nuclide diagram. Note that this differs from Figure S4 because the normalization is for zero additional cover above the bedrock surface.

Figures S7 and S8 show the results of fitting a model with the following exposure history. First, the bedrock surface is the land surface -- there is no sediment cover -- and it erodes at a steady rate for long enough that nuclide concentrations reach a steady state in which production is balanced by nuclide loss via surface erosion and radioactive decay. Second, it is buried under ice for a period of time. This model has two parameters: the steady erosion rate and the burial duration.

The best fit shown in Figures S7 and S8 has steady erosion at 32 m/Myr followed by 1.06 Myr burial. This model does not fit the data as well as Model 1 above; the reduced chi-squared is 5.85 for 5 DOF, implying a probability-of-fit < 0.0001. As seen in Figure S7, this model has difficulty matching both the depth-dependence of the ^{10}Be concentrations and also the ^{26}Al/^{10}Be ratio. Perhaps more importantly, as discussed above, this scenario requires

more than ca. 1 Myr of undisturbed steady erosion prior to burial, which is geologically unlikely in light of evidence for glaciation of Greenland throughout the Pleistocene. In addition, the observation by Bierman and others (2014) of high concentrations of meteoric ^{10}Be in sediment in GISP2 basal ice would be inconsistent with an erosion rate as high as 30 m/Myr. If the sediment analysed by Bierman and others has been buried under ice since 1.1 Ma as our ^{26}Al/^{10}Be ratios indicate, then a steady-state balance calculation based on their Figure 3B would suggest an erosion rate of 7 m/Myr, which would be typical of early Pleistocene cratonic landscapes in North America (Rovey and Balco, 2015). If the erosion rate were 7 m/Myr, we could not match the observed ^{10}Be depth profile with a steady-erosion model unless we also allowed for sediment cover of the bedrock surface. Thus, we conclude that Model 2 is unrealistic and the most likely explanation for the observed depth-dependence of the ^{10}Be and ^{26}Al concentrations is that the present bedrock surface was covered by ~1-4 meters of additional cover at the time that exposure took place.

7. Model 3: Two-stage mixed exposure-erosion scenarios. To complete the discussion of two-stage exposure models, we observe that although we have considered the end members of no erosion with sediment cover and steady-state erosion with no sediment cover (and subsequently rejected the steady-erosion end member), there exist intermediate scenarios that provide an acceptable fit to the data. Here we perform a Monte Carlo simulation in which we consider only two-stage exposure histories with a single period of exposure followed by a single period of burial, but allow the exposure duration, burial duration, erosion rate during exposure, and cover thickness to float. This model is effectively overparameterized and finds many combinations of the parameters that fit the data acceptably well. Here we define 'acceptable' to be reduced chi-squared = 2.6 for 3 DOF, i.e., we cannot reject the model at 95% confidence.

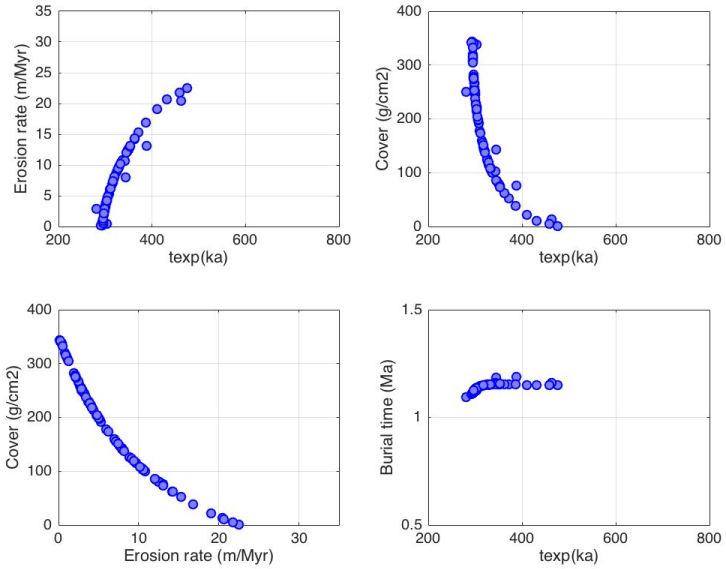

Figure S9. Two-stage exposure-burial models with four adjustable parameters (exposure time, erosion rate during exposure, burial time, and cover of bedrock surface) that yield acceptable fits to the observations.

It is evident from Figure S9 that a wide variety of combinations of exposure time, burial time, and cover of the bedrock surface will adequately fit the observations. Note that the Model 1 scenario is an end member of this distribution. This exercise also demonstrates that the best-fitting burial duration is only very weakly sensitive to the tradeoff between exposure time, erosion rate, and cover thickness. No matter what the exposure time, cover thickness, and erosion rate prior to burial, the observed ^{26}Al/^{10}Be ratio constrains the burial time for any two-stage exposure history to be close to 1.1 Ma.

8. Model 4: Multi-stage exposure-burial scenarios. We now turn to exposure histories with more than two stages. As has been discussed at length in the literature in the context of ^{26}Al - ^{10}Be concentrations observed in bedrock that has been covered by ice in the past (e.g., Bierman and others, 1999), there are an infinite number of possible exposure-burial histories that will yield the observed concentrations and ^{26}Al/^{10}Be ratio. In this case, however, all possible exposure histories share the constraint that at least one period of exposure must have ended no earlier than 1.1 (± 0.1) Ma. If this were not the case -- if the present ice sheet at the core site had been in place for more than 1.1 Ma -- the ^{26}Al/^{10}Be ratio in these samples would be lower than we observe at present. For example, Bierman and others (2014) hypothesized that the GISP2 site has been continuously covered by the Greenland Ice Sheet since 2.7 Ma. Given 350 g/cm^2 of cover of the bedrock surface as discussed above, if this hypothesis were correct, the observed ^{26}Al/^{10}Be concentration in our samples could be no higher than 2.

In this section, therefore, we will propose a series of representative multi-stage exposure-burial scenarios and determine whether or not they are consistent with the observations.

We will also use the observation from Figure S9 above that the burial duration is not sensitive to the particular combination of erosion rate and cover of the bedrock surface during exposure periods to limit the parameter space a bit. Henceforth we will assume that the bedrock surface is covered by 350 g/cm^2 of cover during exposure periods, and the surface erosion rate is zero. If this were not correct, i.e., the erosion rate was greater than zero during exposure periods, this assumption would lead us to slightly underestimate the duration of exposure periods. If we can take the meteoric ^{10}Be measurements of Bierman et al. (2014) as a guide to the likely erosion rate as discussed above, this effect is not significant to any of our conclusions. Note that the significance of underestimating the erosion rate on the inferred duration of exposure periods can be estimated from the upper left panel of Figure S9.

Model 4a: steady-state intermittent exposure-burial.

First, we consider an end member, opposite from the two-stage burial history, in which the site has been cyclically covered and uncovered by ice for long enough that nuclide concentrations have reached a dynamic steady state, in which nuclide production during interglacial periods when the site is exposed is equal to radioactive decay of the existing nuclide inventory during each cycle. We assume 350 g/cm^2 cover and zero erosion as discussed above, we assume 100,000-year glacial-interglacial cycles, and the model has one free parameter: the length of time during each cycle that the site is ice-free. Paleoclimate data, of course, indicate that 100-kyr glacial-interglacial periodicity was not evident prior to ca. 1.2 Ma, so this scenario is only an approximate representation of paleoclimate data. Instead, it represents a simple, but infinitely long, exposure history as a contrast to the shortest possible exposure history that can explain the data (which is Model 1 above).

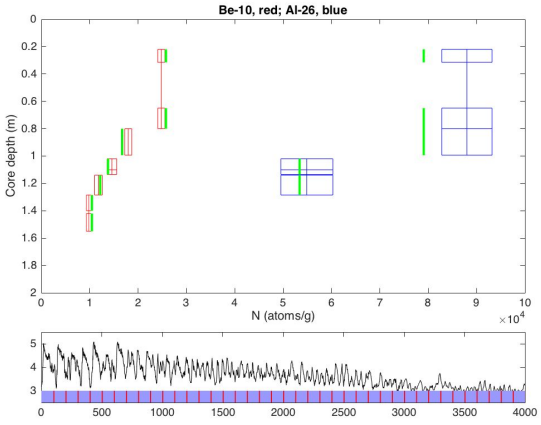

Figure S10. Dynamic steady state model with 100 kyr cycles fit to the data by adjusting the length of interglacials.

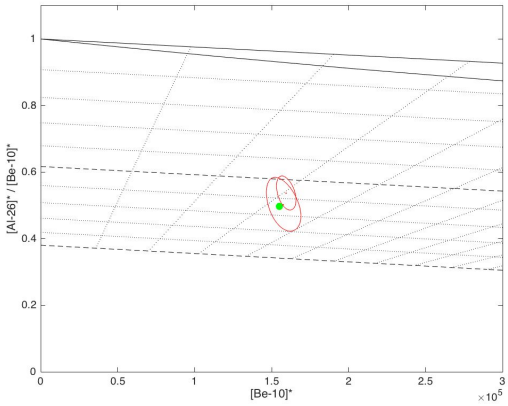

Figure S11. Same exposure history as in Figure S10, on two-nuclide plot.

Interestingly, even though this model has only one fitting parameter (the fraction of each 100 kyr cycle during which the site is ice-free) we can obtain a good fit to the measurements The best-fitting interglacial duration is 8 ka, which fits the data with reduced chi-squared = 1.75 for 6 DOF, i.e. a probability-of-fit of 0.11, which is indistinguishable from the probability-of-fit for Model 1.

Model(s) 4b. Early Pleistocene, or pre-Pleistocene, exposure and some mid-late-Pleistocene interglacials.

Above we have discussed two end-member models that fit the data: a single period of middle Pleistocene exposure followed by 1.1 Myr continuous burial (Model 1; this is the shortest possible exposure model that can fit the data), and a dynamic steady-state model in which the Greenland Ice Sheet is absent for 8 kyr of each 100 kyr glacial-interglacial cycle (Model 4a; as this model is infinitely long, it is the longest possible exposure model that can fit the data, although it is not uniquely so). There are many intermediate models that also fit the data. These are constrained by the general principle that if we start with Model 1 and add any periods of exposure during the most recent 1.1 Myr, then we must also add periods of burial prior to 1.1 Ma to maintain the observed ^{26}Al/^{10}Be ratio. Here we show several

such models in figures S12-S13. All these models have the same probability-of-fit, which is also the same as for Model 1 above (and, in fact, they predict exactly the same ^{26}Al and ^{10}Be concentrations).

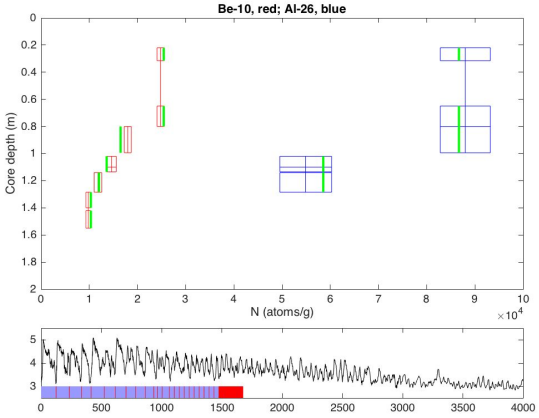

Figure S12. All interglacials during 100-ka glacial-interglacial periodicity after 1.1 Ma, an (arbitrarily long) series of short ice-free interglacials every 41 kyr prior to that, and an initial period of continuous exposure. This model has two fitting parameters: the duration of the long initial exposure period and the duration of the shorter ice-free interglacial periods. The best-fitting duration of the interglacial ice-free periods in this scenario is 4200 years.

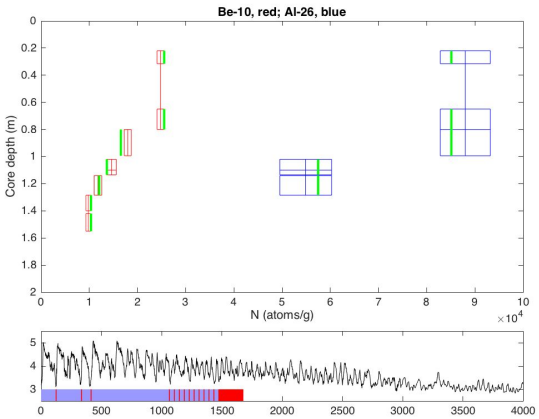

Figure S13. Ice-free conditions during MIS 9, 11, and 13, an arbitrarily long period of short ice-free interglacials during 41 kyr cycles, and a period of continuous mid-Pleistocene exposure. Two adjustable parameters are the same as above. Specifying fewer ice-free periods means they have to be longer; here the best-fitting duration of the interglacial ice-free periods is 7400 years.

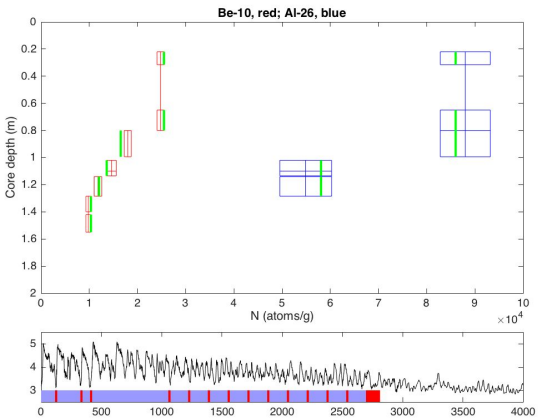

Figure S14. Ice-free conditions during MIS 9, 11, and 13, with occasional ice-free periods in the early Pleistocene. Two adjustable parameters are as above. The best-fitting duration of the short interglacial ice-free periods in this model is 18200 years.

Overall, the important point of these calculations is not that any one of these scenarios is highly likely or favored by other paleoclimate data, but that exposure histories that include ice-free conditions during any or all Pleistocene interglaciations (prior to the present one) can be made to fit the data. However, a scenario in which the present ice sheet has existed continuously for more than the last 1.1 Ma does not fit the observations under any circumstances.

REFERENCES CITED

Balco, G., Stone, J.O., Lifton, N.A. and Dunai, T.J., 2008. A complete and easily accessible means of calculating surface exposure ages or erosion rates from ^{10}Be and ^{26}Al measurements. *Quaternary Geochronology*, *3*(3), pp.174-195.

Balco, G., Briner, J., Finkel, R.C., Rayburn, J.A., Ridge, J.C. and Schaefer, J.M., 2009. Regional beryllium-10 production rate calibration for late-glacial northeastern North America. *Quaternary Geochronology*, *4*(2), pp.93-107.

Bierman, P.R., Marsella, K.A., Patterson, C., Davis, P.T. and Caffee, M., 1999. Mid-Pleistocene cosmogenic minimum-age limits for pre-Wisconsinan glacial surfaces in southwestern Minnesota and southern Baffin Island: a multiple nuclide approach. *Geomorphology*, *27*(1), pp.25-39.

Bierman, P.R., Corbett, L.B., Graly, J.A., Neumann, T.A., Lini, A., Crosby, B.T. and Rood, D.H., 2014. Preservation of a preglacial landscape under the center of the Greenland Ice Sheet. *Science*, *344*(6182), pp.402-405.

Borchers, B., Marrero, S., Balco, G., Caffee, M., Goehring, B., Lifton, N., Nishiizumi, K., Phillips, F., Schaefer, J. and Stone, J., 2016. Geological calibration of spallation production rates in the CRONUS-Earth project.*Quaternary Geochronology*, *31*, pp.188-198.

Chmeleff, J., von Blanckenburg, F., Kossert, K. and Jakob, D., 2010. Determination of the ^{10}Be half-life by multicollector ICP-MS and liquid scintillation counting. *Nuclear Instruments and Methods in Physics Research Section B: Beam Interactions with Materials and Atoms*, *268*(2), pp.192-199.

Heisinger, B., Lal, D., Jull, A.J.T., Kubik, P., Ivy-Ochs, S., Knie, K. and Nolte, E., 2002a. Production of selected cosmogenic radionuclides by muons: 2. Capture of negative muons. *Earth and Planetary Science Letters*, *200*(3), pp.357-369.

Heisinger, B., Lal, D., Jull, A.J.T., Kubik, P., Ivy-Ochs, S., Neumaier, S., Knie, K., Lazarev, V. and Nolte, E., 2002b. Production of selected cosmogenic radionuclides by muons: 1. Fast muons. *Earth and Planetary Science Letters*,*200*(3), pp.345-355.

Korschinek, G., Bergmaier, A., Faestermann, T., Gerstmann, U.C., Knie, K., Rugel, G., Wallner, A., Dillmann, I., Dollinger, G., Von Gostomski, C.L. and Kossert, K., 2010. A new value for the half-life of ^{10}Be by heavy-ion elastic recoil detection and liquid scintillation counting. *Nuclear Instruments and Methods in Physics Research Section B: Beam Interactions with Materials and Atoms*, *268*(2), pp.187-191.

Lisiecki, L.E. and Raymo, M.E., 2005. A Pliocene-Pleistocene stack of 57 globally distributed benthic δ^{18}O records. *Paleoceanography*, *20*(1).

Nishiizumi, K., 2004. Preparation of ^{26}Al AMS standards. *Nuclear Instruments and Methods in Physics Research Section B: Beam Interactions with Materials and Atoms*, *223*, pp.388-392.

Phillips, F.M., Argento, D.C., Balco, G., Caffee, M.W., Clem, J., Dunai, T.J., Finkel, R., Goehring, B., Gosse, J.C., Hudson, A.M. and Jull, A.T., 2016. The CRONUS-Earth project: a synthesis. *Quaternary Geochronology*, *31*, pp.119-154.

Rovey, C.W. and Balco, G., 2015. Paleoclimatic interpretations of buried paleosols within the pre-Illinoian till sequence in northern Missouri, USA.*Palaeogeography, Palaeoclimatology, Palaeoecology*, *417*, pp.44-56.

Stone, J.O., 2000. Air pressure and cosmogenic isotope production. *Journal of Geophysical Research: Solid Earth*, *105*(B10), pp.23753-23759.